Research Square

Preprints are preliminary reports that have not undergone peer review.
They should not be considered conclusive, used to inform clinical practice,
or referenced by the media as validated information.

Widespread synchronous decline in a Mediterranean forest driven by accelerated aridity

Alejandro Miranda (mirandac.alejandro@gmail.com)
Universidad de Chile https://orcid.org/0000-0002-8211-0179

Juan Ovalle
Universidad de Chile

Alexandra Syphard
Conservation Biology Institute

Miguel Berdugo
ETH https://orcid.org/0000-0003-1053-8907

Jaime Carrasco
Universidad de Chiel

Rayen Mentler
Center for Climate and Resilience Research (CR2)

Francisco Squeo
Universidad de La Serena

Cristian Delpiano
Universidad de La Serena

Solange Vargas
Universidad de La Serena

Marcelo Miranda
Pontificia Universidad Católica de Chile

Cynnamon Dobbs
Centro de Modelacion y Monitoreo de Ecosistemas, Facultad de Ciencias, Universidad Mayor

Susana Gómez-González
Universidad de Cádiz

Antonio Lara
Laboratorio de Dendrocronología y Cambio Global, Universidad Austral de Chile

Rene D. Garreaud
University of Chile

Brief Communication

Keywords:

Posted Date: June 22nd, 2022

DOI: https://doi.org/10.21203/rs.3.rs-1769566/v1

License: This work is licensed under a Creative Commons Attribution 4.0 International License.
Read Full License

Widespread synchronous decline in a Mediterranean forest driven by accelerated aridity

Abstract:

Ecosystem collapse in direct response to climate change is a critical but poorly documented phenomenon. By assessing the climate context and productivity trends in Mediterranean ecosystems worldwide, we found a large-scale, abrupt forest decline in Chile (>90% in <100 days) as response to a sustained, acute drought unprecedented in the recent history of Mediterranean-type ecosystems. These extreme conditions were projected for 2070-2090, suggesting that climate change impacts are accelerating.

Main text

Ecosystem collapse (EC) involves an abrupt transition beyond the threshold of natural variability, fundamentally altering one or more of the ecosystem's characteristics (*1–3*). Recent increases in climate-induced tree mortality raises concern that some forest ecosystems are on the brink of collapse across wide environmental gradients (*4*, *5*). Long-lasting, decadal and/or intense droughts are potential drivers of macro-scale ecosystem degradation and collapse (*6*). However, since droughts of such extremity have rarely occurred, their capacity to drive significant biodiversity shifts remains largely unknown (*6*). Therefore, assessments of climate-driven ecosystem change mostly rely on space-for-time substitution approaches, results from which are difficult to validate or reproduce findings over time (*7*).

The shrublands and forests from the world's five Mediterranean-type ecosystems (MTEs; Fig. S1) are especially important to monitor for ecosystem change signs because they border semiarid and desert ecosystems, being thus potentially vulnerable to hot drought-driven EC. Although woody species of MTEs are adapted to low soil water potential (*8*), changes in climatic extremes may exceed species physiological tolerances (*9–11*). The socio-ecological impacts of EC in MTEs could be elevated considering that they are biodiversity hotspots and host ~500 million people (*8*). Understanding the direct role of climate change on regional EC is crucial to develop adaptation and mitigation programs that reduce its impacts on biodiversity and society's well-being. Here, we analyzed the trends of forest productivity and its climatic context in the last decades across the world's five MTEs to investigate signs of EC.

Satellite-based Normalized Difference Vegetation Index (NDVI) time series were used as a surrogate for dominant tree layer photosynthetic productivity or greenness (*12*, *13*), to assess 21 years of change in 111,170 Km^2 of MTEs forests worldwide (Table S1). We found no significant negative trends in the regional average, annual mean NDVI in all MTEs but for central Chile. In 2020 it experienced the lowermost NDVI values and largest negative anomalies of all MTEs in the last two decades pushing the system well below its natural variability range for 2000–2010 (Fig. 1A). We also observed some local negative NDVI trends between 2000-2021 in other MTEs localities (individual pixel analysis) ($p < 0.01$) of California, Southwest Australia, South Africa, and the Mediterranean Basin, affecting 8.3%, 6%, 5.7%, and 1% of the forest area, respectively. The same trend analysis shows a 39% of individual pixel with negative trend in Chile revealing the largest impacted area despite being the least extensive MTEs (Table S1). A detailed analysis for central Chile revealed that in late 2019, more than 90% of the region's forest area showed an abrupt, synchronous decline (mean and maximum anomaly, respectively -29,6% and -57% of 2018 values; Fig. 1B). These abrupt changes started within 100 days (May–June) for 82.4% of the forest area affected, thus being synchronous in time (Fig. 1B). Moreover, these changes occurred across a latitudinal range of ~500 km, and ~120 km from the coastal to Andean range, under different local environmental conditions, species composition, structure, dominance, and degradation history (Fig. 1B).

Except for the Mediterranean Basin, the last decade (2010–2021) was drier than average in all MTEs, with mean deficits ranging from -2% (Southwest Australia) to -28% (central Chile; Fig. 2A). Dry years were dominant but were interspersed with wet years for all MTEs except for central Chile, where all years since 2010 were below average (Fig. 2A). This conforms the so-called mega drought affecting a large portion of central-southern Chile (beyond the MTE sector), resulting in the driest decade in local history since at least the 14^{th} century (*14*) and for any MTEs since 1901 (Fig. 2B). Moreover, 2011-2021 was the warmest registered decade for all

MTEs (Fig. 2B), leading to a negative trend in decadal surface water balance expressed as the Standardized Precipitation-Evapotranspiration Index (SPEI-12; Fig. S2).

The climatic anomalies during the last decade in the five MTEs are broadly consistent with projections from coupled general circulation models (*15*). In central Chile, however, natural variability originating in the subtropical southwest Pacific was conducive for dry conditions across the Pacific (*16*), acting synchronously with the climate-change signal. As a result, the observed mean precipitation deficit (~30% of the long-term historical mean) was about three times larger than expected for the early decades of the 21st century, more akin to those predicted for 2070-2090 under a heavy GHG emission scenario (Fig. 2A) (*17*). The central Chile mega drought also encompasses 2019 when the region received less than 30% of the mean rainfall (Fig. 1B) accompanied by record high temperatures in spring/summer (*18*). This extremely dry and warm year, termed 'hyper-drought' during the decade-long mega-drought, was likely responsible for this sudden and massive canopy collapse that may constitute one of the most notable examples of direct climate driven impact on the recent history of MTEs (Fig. 1A).

To further investigate local dependencies of observed forest decline, we complemented satellite observations with field measurements of leaf area index (LAI) during 2017–2020 for 474 trees in 78 plots of the four most abundant forest species of central Chile. We documented responses of species adapted to mesic conditions (*Cryptocarya alba* and *Peumus boldus)* and xeric conditions (*Quillaja saponaria* and *Lithaea caustica*). LAI analysis confirmed a widespread trend of decreasing productivity, with the most intense decline in trees adapted to more mesic conditions (Fig. S3). The distribution of tree crown decay percentage of species groups was bi-modal, indicating higher densities of trees with both low-level (0–25%) and high-level (75–100%) canopy damage (Fig. S4). This differential response could indicate a yet unknown specific physiological mechanism, micro-site condition, or density-dependent process that imparts selective resilience to sustained hot-droughts. This also may suggest a rapid massive decline with little intermediate effect (Fig. S4), which could produce significant changes in community composition. In general, extreme drought increases the risk of hydraulic failure and carbon starvation (*10*, *11*), but failure of the plant hydraulic system is likely the main mechanism involved in extensive canopy death (*11*). This mechanism may be particularly relevant for evergreen species that exhibit comparatively lower wood density and higher specific leaf area (*19*).

Although regrowth from underground structures is potentially possible given sufficient carbon stocks, recovery of these forests is uncertain under persistent drought with water balance continually decreasing. Model simulations under heavy GHG emission scenarios consistently predict aridification of MTEs, with precipitation reduction of up to 40% over the 21st century (*15*). In California and Mediterranean basin has already reported increased large-scale tree mortality and shrubland dieback under recent persistent droughts (*20*, *21*). In Southwest Australia, after local sudden canopy collapse of eucalypt forest, experienced a 26% of stem mortality after collapse (28). There still scarce impact evidence of the massive 2020 sudden decline in Chile, however it has reported that large-scale browning may represent an increasing risk of wildfires (*22*), that combined with hot-drought condition may arrest natural recovery pushing the ecosystem to a new stable-state condition (*23*). Also, slow tree growth in the last decade (*24*) reflect a decreasing atmospheric carbon uptake by the forest. All these factors operating simultaneously could contribute as a positive feedback to the rapid aridification and shifting of this MTE, facilitating disturbances that further promote EC (*25*).

In terrestrial ecosystems, direct climate-driven collapse manifests primarily as local state changes at limited geographical extents, such as vegetation type conversion, local extinction, or extensive tree mortality (*26*). The relatively fewer examples of regional-scale collapse mostly result from indirect effects of extreme and punctual climate-driven changes, such as insect outbreaks, altered fire regimes, floods, storms, or changes in sea level (*4*, *5*, *25*, *26*). At the local scale, climate-induced forest/tree decline exhibited a patchy spatial pattern determined by plant age, species traits and demographics, disturbance response and composition in combination with, or interacting with, site variability e.g., soil properties and topography (*4*, *5*). Large-scale, direct climate-driven process are rare but reveals the potential impact of sustained climate change (*6*, *27*). As for other MTEs, historical land-use change in central Chile has restricted most of the remnant forests to slopes with limited access to groundwater. This would explain the synchronous decline caused from exceeding the critical threshold of forest water potential, with reduced effect in ravine bottoms (*28*).

Vegetation productivity decline manifested in decreasing NDVI could be the primary ecosystem response to increasing aridity and the first step in a cascade of abrupt changes affecting other ecosystem functions and attributes, hampering nature's contribution to people (*7*). Studies suggest that long-term reduction in productivity and survival of Mediterranean species could reach a tipping point, leading to abrupt, irreversible changes in ecosystem functioning (*7*, *21*). Greater efforts are required for understanding the mechanisms behind ecological change, its impacts, and the safe operating space for socio-ecological system functioning to prepare for a rapidly changing earth system (*29*, *30*). The types of climate anomalies and impacts observed in the last decade in central Chile, suggest that climate change effects are occurring sooner than expected and may be a spyglass to the future for other MTEs.

Figures

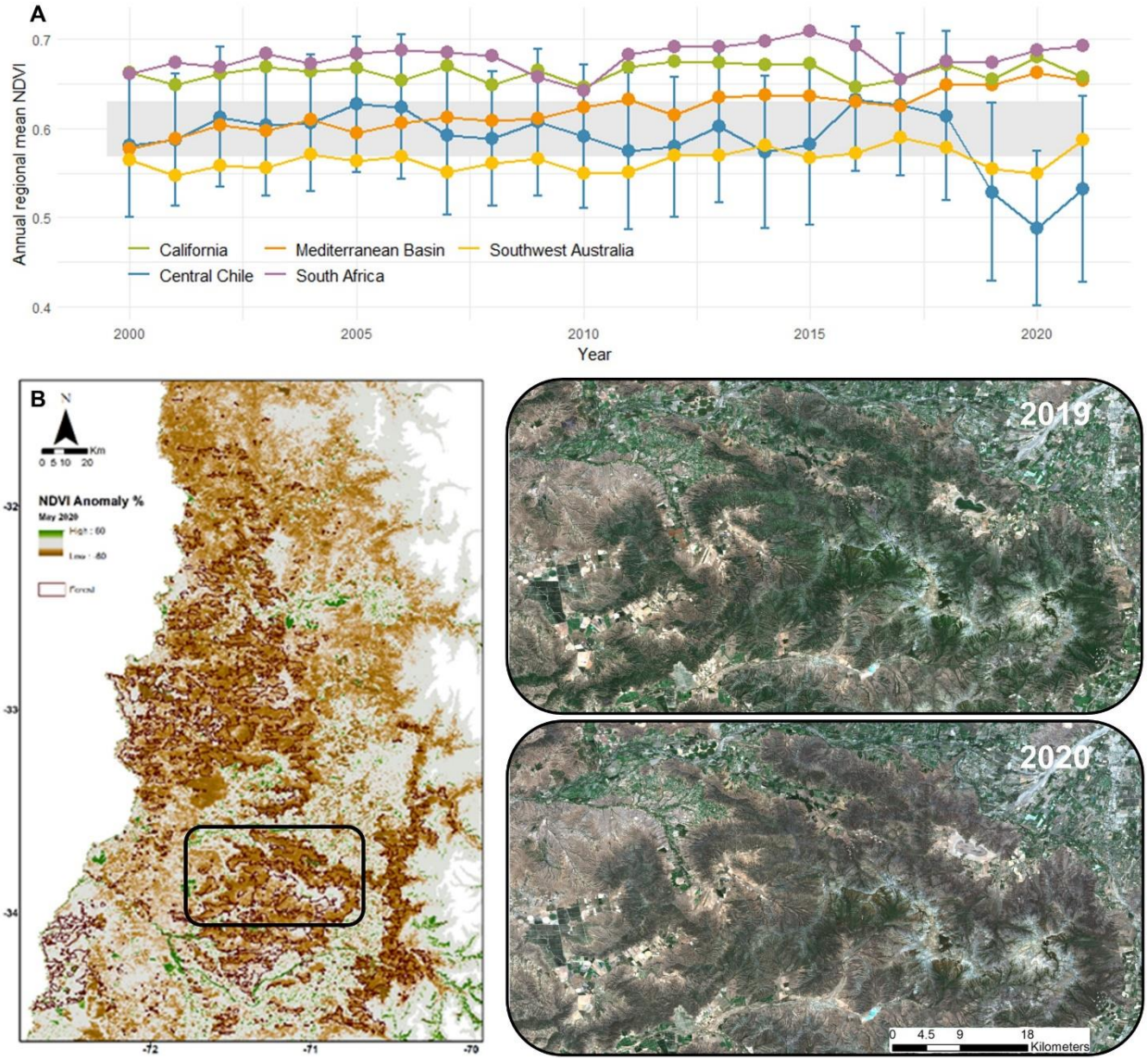


Figure 1. **Annual regional mean NDVI change for all MTEs and NDVI anomaly for central Chile. (A)** The absolute annual variation of NDVI for each MTEs, representing the mean NDVI value for the entire year, for every forest stand and then the regional mean NDVI was calculated as the mean of the stand annual means. The gray band represents the regional annual mean±2SD for central Chile for 2000–2010 over the same period as a pre-mega-drought decadal variability in NDVI values. Error bars for central Chile indicate the all-season variability for every forest stand in the region. **(B)** NDVI anomaly for May 2020 compared with the mean value for the same month for 2000–2010. Left panels are Sentinel-2 true color representation of the southern part of central Chile (45 km × 70 km) showing the browning effect between 2019 and 2020.

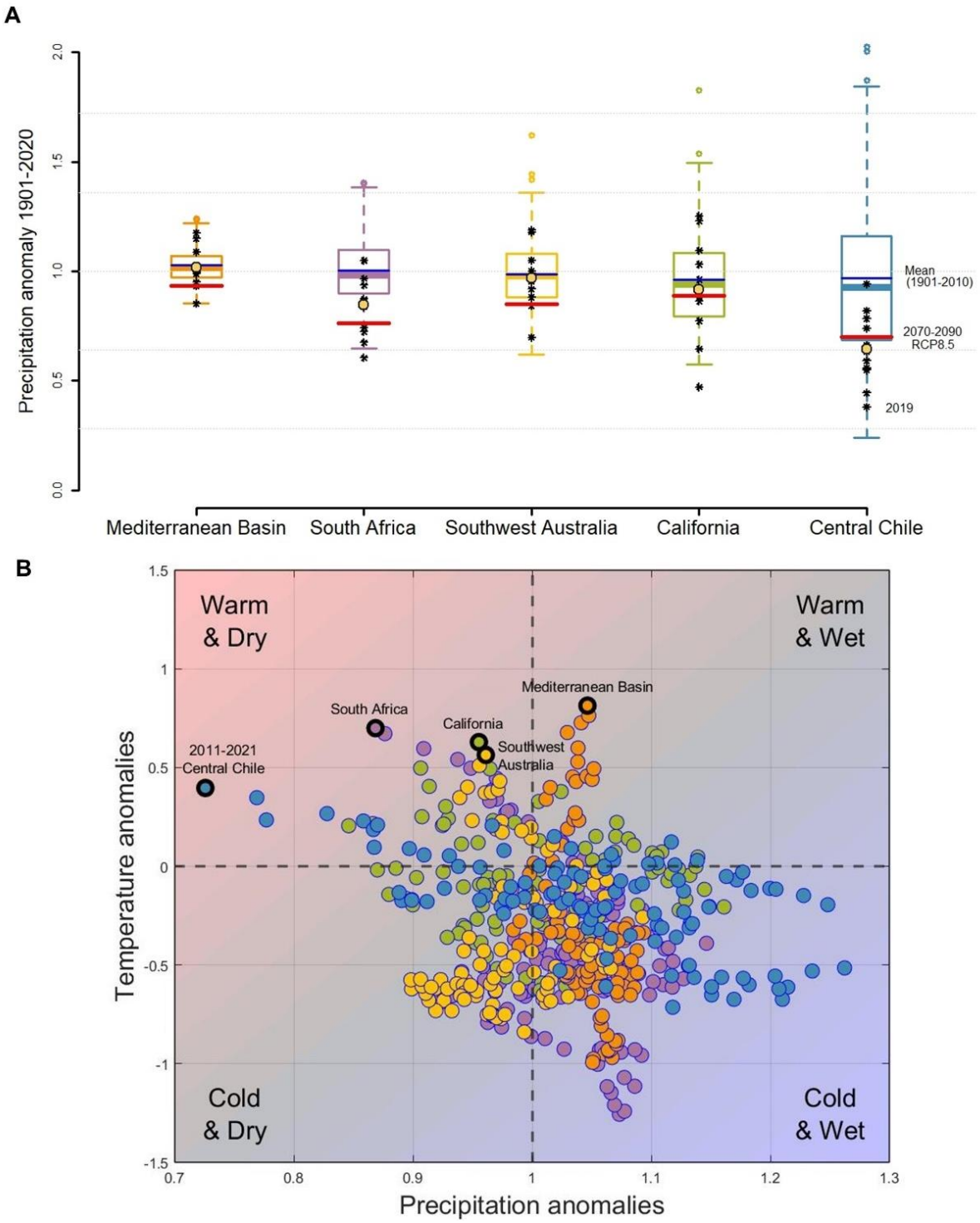


Figure 2. MTEs precipitation and temperature anomaly's. (**A**) Boxplot of the annual precipitation in each MTE considering the period 1901-2020 using CRU data. All values are expressed as fraction relative to the long-term mean value (1901-2010, thick value in each box). The upper (lower) limit of the boxes correspond to the 75% (25%) quantile. Black asterisks show individual annual precipitation anomalies for the period 2010–2020 and yellow circles indicate the 2010–2020 mean. Red lines indicate the expected value of average precipitation anomaly for 2070–2090 under RCP8.5. (B) Plot of decadal temperature and precipitation for the five MTEs for 1901–2021 with decadal averages for 2011–2021 outlined in black. The precipitation series were standardized (dividing by the climatology) to allow comparison among the MTEs. Likewise, the temperature anomalies correspond to the decadal values minus the long-term climatology.

References and Notes

1. D. M. Bergstrom *et al.*, *Glob. Change Biol.* **27**, 1692–1703 (2021).
2. L. M. Bland *et al.*, *Front. Ecol. Environ.* **16**, 29–36 (2018).
3. A. C. Newton *et al.*, *Biol. Conserv.* **264**, 109366 (2021).
4. C. D. Allen, D. D. Breshears, N. G. McDowell, *Ecosphere*. **6** (2015), doi:10.1890/ES15-00203.1.
5. C. D. Allen *et al.*, *For. Ecol. Manag.* **259**, 660–684 (2010).
6. R. C. Godfree *et al.*, *Proc. Natl. Acad. Sci.* **116**, 15580–15589 (2019).
7. M. Berdugo *et al.*, *Science*. **367**, 787–790 (2020).
8. P. W. Rundel *et al.*, *Annu. Rev. Ecol. Syst.* **47**, 387–407 (2016).
9. W. R. L. Anderegg, L. D. L. Anderegg, K. L. Kerr, A. T. Trugman, *Glob. Change Biol.* **25**, 3793–3802 (2019).
10. H. D. Adams *et al.*, *Nat. Ecol. Evol.* **1**, 1285–1291 (2017).
11. B. Choat *et al.*, *Nature*. **558**, 531–539 (2018).
12. A. J. Das *et al.*, *Ecol. Appl.* **32** (2022), doi:10.1002/eap.2514.
13. N. Pettorelli *et al.*, *Trends Ecol. Evol.* **20**, 503–510 (2005).
14. R. D. Garreaud *et al.*, *Int. J. Climatol.* (2019), doi:10.1002/joc.6219.
15. IPCC, Climate Change 2021: The Physical Science Basis. Contribution of Working Group I to the Sixth Assessment Report of the Intergovernmental Panel on Climate Change (2021), (available at https://www.ipcc.ch/report/ar6/wg1/#FullReport).
16. R. D. Garreaud, K. Clem, J. V. Veloso, *J. Clim.* **34**, 7661–7676 (2021).
17. D. Bozkurt, M. Rojas, J. P. Boisier, J. Valdivieso, *Clim. Change*. **150**, 131–147 (2018).
18. M. T. K. Arroyo *et al.*, *Plants*. **9**, 1553 (2020).
19. E. Andivia *et al.*, *Ecol. Appl.* **31**, 1–11 (2021).
20. C. J. Fettig, L. A. Mortenson, B. M. Bulaon, P. B. Foulk, *For. Ecol. Manag.* **432**, 164–178 (2019).
21. C. Senf, A. Buras, C. S. Zang, A. Rammig, R. Seidl, *Nat. Commun.* **11**, 1–8 (2020).
22. R. O. Chávez *et al.*, *Front. Environ. Sci.* **10**, 865406 (2022).

23. C. Smith-Ramírez *et al.*, *For. Ecol. Manag.* **485**, 118922 (2021).

24. A. Venegas-González *et al.*, *Ecosystems* (2022), doi:10.1007/s10021-022-00760-x.

25. R. Seidl *et al.*, *Nat. Clim. Change*. **7**, 395–402 (2017).

26. A. C. Newton, *Ecosystem Collapse and Recovery* (Cambridge University Press, ed. 1, 2021; https://www.cambridge.org/core/product/identifier/9781108561105/type/book).

27. S. Saatchi *et al.*, *Proc. Natl. Acad. Sci.* **110**, 565–570 (2013).

28. A. Miranda *et al.*, *Ecol. Indic.* **115** (2020), doi:10.1016/j.ecolind.2020.106401.

29. J. Dudney, K. N. Suding, *Nat. Ecol. Evol.* **4**, 1449–1450 (2020).

30. H. Hillebrand *et al.*, *Nat. Ecol. Evol.* **4**, 1502–1509 (2020).

Supplementary Files

This is a list of supplementary files associated with this preprint. Click to download.

- MirandaetalGlobMedSupplementaryMaterials17062022blind.pdf